

# 16

## Moiré and Fringe Projection Techniques

*K. Creath and J. C. Wyant*

### 16.1. INTRODUCTION

The term “moiré” is not the name of a person; in fact, it is a French word referring to “an irregular wavy finish usually produced on a fabric by pressing between engraved rollers” (Webster's 1981). In optics it refers to a beat pattern produced between two gratings of approximately equal spacing. It can be seen in everyday things such as the overlapping of two window screens, the rescreening of a half-tone picture, or with a striped shirt seen on television. The use of moiré for reduced sensitivity testing was introduced by Lord Rayleigh in 1874. Lord Rayleigh looked at the moiré between two identical gratings to determine their quality even though each individual grating could not be resolved under a microscope.

Fringe projection entails projecting a fringe pattern or grating on an object and viewing it from a different direction. The first use of fringe projection for determining surface topography was presented by Rowe and Welford in 1967. It is a convenient technique for contouring objects that are too coarse to be measured with standard interferometry. Fringe projection is related to optical triangulation using a single point of light and light sectioning where a single line is projected onto an object and viewed in a different direction to determine the surface contour (Case et al. 1987).

Moiré and fringe projection interferometry complement conventional holographic interferometry, especially for testing optics to be used at long wavelengths. Although two-wavelength holography (TWH) can be used to contour surfaces at any longer-than-visible wavelength, visible interferometric environmental conditions are required. Moiré and fringe projection interferometry can contour surfaces at any wavelength longer than 10-100  $\mu\text{m}$  with reduced environmental requirements and no intermediate photographic recording setup.

Moiré is also a useful technique for aiding in the understanding of interferometry.

This chapter explains what moiré is and how it relates to interferometry. Contouring techniques utilizing fringe projection, projection and shadow moiré, and two-angle holography are all described and compared. Each of these techniques provides the same result and can be described by a single theory. The relationship between these techniques and holographic and conventional interferometry will be shown. Errors caused by divergent geometries are described, and applications of these techniques combined with phase measurement techniques are presented. Further information on these techniques can be found in the following books and book chapters: Varner (1974), Vest (1979), Hariharan (1984), Gasvik (1987), and Chiang (1978, 1983).

## 16.2. WHAT IS MOIRÉ?

Moiré patterns are extremely useful to help understand basic interferometry and interferometric test results. Figure 16.1 shows the moiré pattern (or beat pattern) produced by two identical straight-line gratings rotated by a small angle relative to each other. A dark fringe is produced where the dark lines are out of step one-half period, and a bright fringe is produced where the dark lines for one grating fall on top of the corresponding dark lines for the second grating. If the angle between the two gratings is increased, the separation between the bright and dark fringes decreases. [A simple explanation of moiré is given by Oster and Nishijima (1963).]

If the gratings are not identical straight-line gratings, the moiré pattern (bright and dark fringes) will not be straight equi-spaced fringes. The following anal-

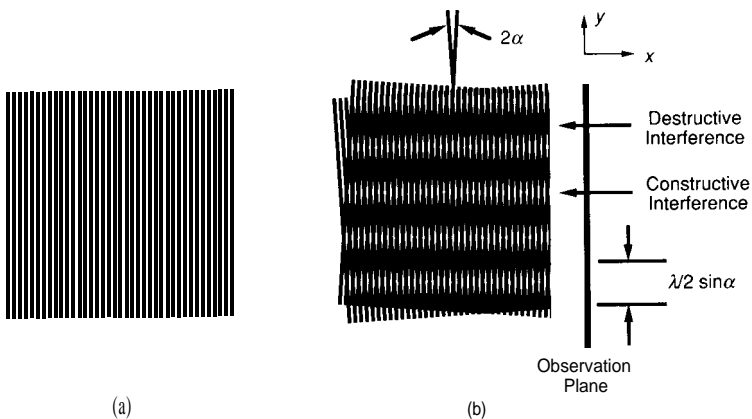


**Figure 16.1.** (a) Straight-line grating. (b) Moiré between two straight-line gratings of the same pitch at an angle  $\alpha$  with respect to one another.

ysis shows how to calculate the moire pattern for arbitrary gratings. Let the intensity transmission function for two gratings  $f_1(x, y)$  and  $f_2(x, y)$  be given by

$$\begin{aligned} f_1(x, y) &= a_1 + \sum_{n=1}^{\infty} b_{1n} \cos [n\phi_1(x, y)], \\ f_2(x, y) &= a_2 + \sum_{m=1}^{\infty} b_{2m} \cos [m\phi_2(x, y)], \end{aligned} \quad (16.1)$$

where  $\phi(x, y)$  is the function describing the basic shape of the grating lines. For the fundamental frequency,  $\phi(x, y)$  is equal to an integer times  $2\pi$  at the center of each bright line and is equal to an integer plus one-half times  $2\pi$  at the center of each dark line. The  $b$  coefficients determine the profile of the grating lines (i.e., square wave, triangular, sinusoidal, etc.) For a sinusoidal line profile,  $b_{11}$  is the only nonzero term.

When these two gratings are superimposed, the resulting intensity transmission function is given by the product

$$\begin{aligned} f_1(x, y) f_2(x, y) &= a_1 a_2 + a_1 \sum_{m=1}^{\infty} b_{2m} \cos [m\phi_2(x, y)] \\ &\quad + a_2 \sum_{n=1}^{\infty} b_{1n} \cos [n\phi_1(x, y)] \\ &\quad + \sum_{m=1}^{\infty} \sum_{n=1}^{\infty} b_{1n} b_{2m} \cos [n\phi_1(x, y)] \cos [m\phi_2(x, y)]. \end{aligned} \quad (16.2)$$

The first three terms of Eq. (16.2) provide information that can be determined by looking at the two patterns separately. The last term is the interesting one, and can be rewritten as

$$\begin{aligned} \text{Term 4} &= \frac{1}{2} b_{11} b_{21} \cos [\phi_1(x, y) - \phi_2(x, y)] \\ &\quad + \frac{1}{2} \sum_{m=1}^{\infty} \sum_{n=1}^{\infty} b_{1n} b_{2m} \cos [n\phi_1(x, y) - m\phi_2(x, y)]; \\ &\quad n \text{ and } m \text{ both } \neq 1 \\ &\quad + \frac{1}{2} \sum_{m=1}^{\infty} \sum_{n=1}^{\infty} b_{1n} b_{2m} \cos [n\phi_1(x, y) + m\phi_2(x, y)]. \end{aligned} \quad (16.3)$$

This expression shows that by superimposing the two gratings, the sum and difference between the two gratings is obtained. The first term of Eq. (16.3)

represents the difference between the fundamental pattern masking up the two gratings. It can be used to predict the moiré pattern shown in Fig. 16.1. Assuming that two gratings are oriented with an angle  $2\alpha$  between them with the  $y$  axis of the coordinate system bisecting this angle, the two grating functions  $\phi_1(x, y)$  and  $\phi_2(x, y)$  can be written as

$$\phi_1(x, y) = \frac{2\pi}{\lambda_1} (x \cos \alpha + y \sin \alpha)$$

and

$$\phi_2(x, y) = \frac{2\pi}{\lambda_2} (x \cos \alpha - y \sin \alpha), \quad (16.4)$$

where  $\lambda_1$  and  $\lambda_2$  are the line spacings of the two gratings. Equation (16.4) can be rewritten as

$$\phi_1(x, y) - \phi_2(x, y) = \frac{2\pi}{\lambda_{\text{beat}}} x \cos \alpha + \frac{4\pi}{\lambda} y \sin \alpha, \quad (16.5)$$

where  $\bar{\lambda}$  is the average line spacing, and  $\lambda_{\text{beat}}$  is the beat wavelength between the two gratings given by

$$\lambda_{\text{beat}} = \frac{\lambda_1 \lambda_2}{\lambda_2 - \lambda_1}. \quad (16.6)$$

Note that this beat wavelength equation is the same as that obtained for two-wavelength interferometry as shown in Chapter 15. Using Eq. (16.3), the moiré or beat will be lines whose centers satisfy the equation

$$\phi_1(x, y) - \phi_2(x, y) = M2\pi. \quad (16.7)$$

Three separate cases for moiré fringes can be considered. When  $\lambda_1 = \lambda_2 = \lambda$ , the first term of Eq. (16.5) is zero, and the fringe centers are given by

$$M\lambda = 2y \sin \alpha, \quad (16.8)$$

where  $M$  is an integer corresponding to the fringe order. As was expected, Eq. (16.8) is the equation of equi-spaced horizontal lines as seen in Fig. 16.1. The other simple case occurs when the gratings are parallel to each other with  $\alpha = 0$ . This makes the second term of Eq. (16.5) vanish. The moiré will then be lines that satisfy

$$M\lambda_{\text{beat}} = x. \quad (16.9)$$

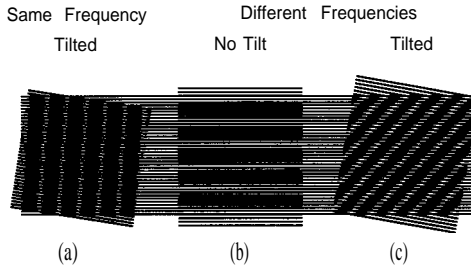


Figure 16.2. Moiré patterns caused by two straight-line gratings with (a) the same pitch tilted with respect to one another, (b) different frequencies and no tilt, and (c) different frequencies tilted with respect to one another.

These fringes are equally spaced, vertical lines parallel to the  $y$  axis. For the more general case where the two gratings have different line spacings and the angle between the gratings is nonzero, the equation for the moiré fringes will now be

$$M\bar{\lambda} = \frac{\bar{\lambda}}{\lambda_{\text{beat}}} x \cos \alpha + 2y \sin \alpha. \tag{16.10}$$

This is the equation of straight lines whose spacing and orientation is dependent on the relative difference between the two grating spacings and the angle between the gratings. Figure 16.2 shows moiré patterns for these three cases.

The orientation and spacing of the moiré fringes for the general case can be determined from the geometry shown in Fig. 16.3 (Chiang, 1983). The distance  $AB$  can be written in terms of the two grating spacings;

$$\overline{AB} = \frac{\lambda_1}{\sin(\theta - \alpha)} = \frac{\lambda_2}{\sin(\theta + \alpha)}, \tag{16.11}$$

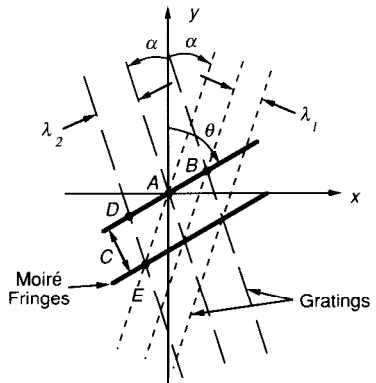


Figure 16.3. Geometry used to determine spacing and angle of moiré fringes between two gratings of different frequencies tilted with respect to one another.

where  $\theta$  is the angle the moiré fringes make with the y axis. After rearranging, the fringe orientation angle  $\theta$  is given by

$$\tan \theta = \tan \alpha \left( \frac{\lambda_1 + \lambda_2}{\lambda_2 - \lambda_1} \right). \quad (16.12)$$

When  $\alpha = 0$  and  $\lambda_1 \neq \lambda_2$ ,  $\theta = 0^\circ$  and when  $\lambda_1 = \lambda_2$  with  $\alpha \neq 0$ ,  $\theta = 90^\circ$  as expected. The fringe spacing perpendicular to the fringe lines can be found by equating quantities for the distance **DE**;

$$\overline{DE} = \frac{\lambda_1}{\sin 2\alpha} = \frac{C}{\sin(\theta + \alpha)}, \quad (16.13)$$

where C is the fringe spacing or contour interval. This can be rearranged to yield

$$C = \lambda_1 \left[ \frac{\sin(\theta + \alpha)}{\sin 2\alpha} \right]. \quad (16.14)$$

By substituting for the fringe orientation  $\theta$ , the fringe spacing can be found in terms of the grating spacings and angle between the gratings;

$$C = \frac{\lambda_1 \lambda_2}{\sqrt{\lambda_2^2 \sin^2 2\alpha + (\lambda_2 \cos 2\alpha - \lambda_1)^2}}. \quad (16.15)$$

In the limit that  $\alpha = 0$  and  $\lambda_1 \neq \lambda_2$ , the fringe spacing equals  $\lambda_{\text{beat}}$ , and in the limit that  $\lambda_1 = \lambda_2 = \lambda$  and  $\alpha \neq 0$ , the fringe spacing equals  $\lambda/(2 \sin \alpha)$ . It is possible to determine  $\lambda_2$  and  $\alpha$  from the measured fringe spacing and orientation as long as  $\lambda_1$  is known (Chiang 1983).

### 16.3. MOIRÉ AND INTERFEROGRAMS

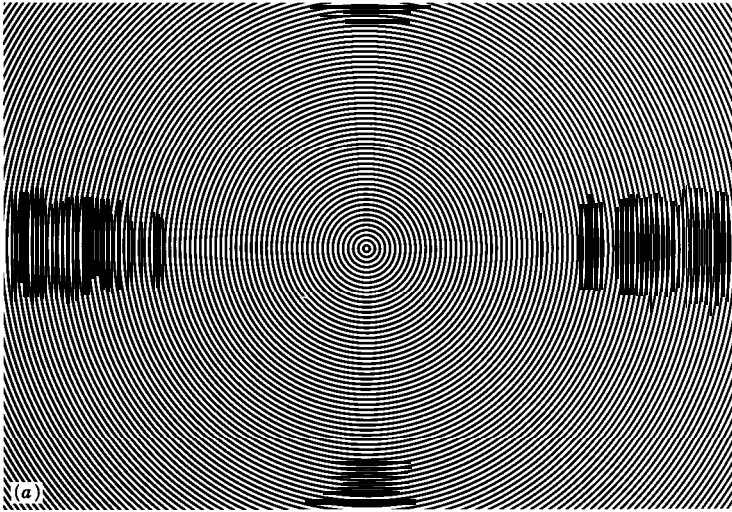
Now that we have covered the basic mathematics of moiré patterns, let us see how moiré patterns are related to interferometry. The single grating shown in Fig. 16.1 can be thought of as a “snapshot” of a plane wave traveling to the right, where the distance between the grating lines is equal to the wavelength of light. The straight lines represent the intersection of a plane of constant phase with the plane of the figure. Superimposing the two sets of grating lines in Fig. 16.1 can be thought of as superimposing two plane waves with an angle of  $2\alpha$  between their directions of propagation. Where the two waves are in phase, bright fringes result (constructive interference), and where they are out of phase,

dark fringes result (destructive interference). For a plane wave, the “grating” lines are really planes perpendicular to the plane of the figure and the dark and bright fringes are also planes perpendicular to the plane of the figure. If the plane waves are traveling to the right, these fringes would be observed by placing a screen perpendicular to the plane of the figure and to the right of the grating lines as shown in Fig. 16.1. The spacing of the interference fringes on the screen is given by Eqn. (16.8), where  $\lambda$  is now the wavelength of light. Thus, the moiré of two straight-line gratings correctly predicts the centers of the interference fringes produced by interfering two plane waves. Since the gratings used to produce the moiré pattern are binary gratings, the moiré does not correctly predict the sinusoidal intensity profile of the interference fringes. (If both gratings had sinusoidal intensity profiles, the resulting moiré would still not have a sinusoidal intensity profile because of higher-order terms.)

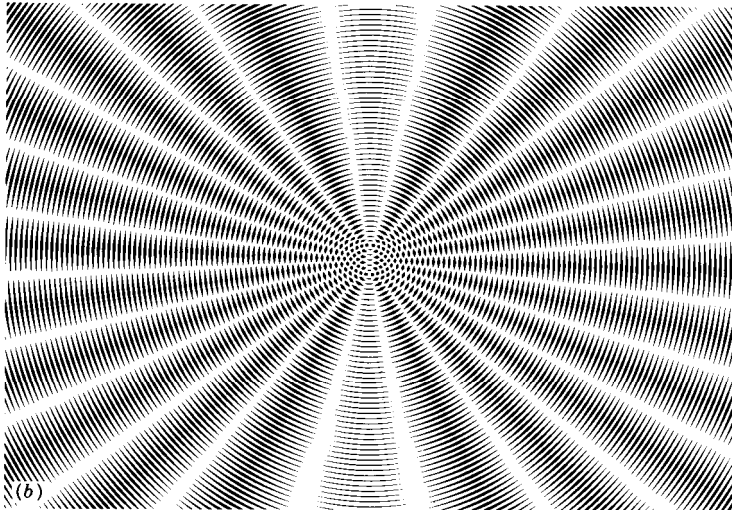
More complicated gratings, such as circular gratings, can also be investigated. Figure 16.4b shows the superposition of two circular line gratings. This pattern indicates the fringe positions obtained by interfering two spherical wavefronts. The centers of the two circular line gratings can be considered the source locations for two spherical waves. Just as for two plane waves, the spacing between the grating lines is equal to the wavelength of light. When the two patterns are in phase, bright fringes are produced; and when the patterns are completely out of phase, dark fringes result. For a point on a given fringe, the difference in the distances from the two source points and the fringe point is a constant. Hence, the fringes are hyperboloids. Due to symmetry, the fringes seen on observation plane *A* of Fig. 16.4b must be circular. (Plane *A* is along the top of Fig. 16.4b and perpendicular to the line connecting the two sources as well as perpendicular to the page.) Figure 16.4c shows a binary representation of these interference fringes and represents the interference pattern obtained by interfering a nontilted plane wave and a spherical wave. (A plane wave can be thought of as a spherical wave with an infinite radius of curvature.) Figure 16.4d shows that the interference fringes in plane *B* are essentially straight equi-spaced fringes. (These fringes are still hyperbolas, but in the limit of large distances, they are essentially straight lines. Plane *B* is along the side of Fig. 16.4b and parallel to the line connecting the two sources as well as perpendicular to the page.)

The lines of constant phase in plane *B* for a single spherical wave are shown in Fig. 16.5a. (To first-order, the lines of constant phase in plane *B* are the same shape as the interference fringes in plane *A*.) The pattern shown in Fig. 16.5a is commonly called a zone plate. Figure 16.5b shows the superposition of two linearly displaced zone plates. The resulting moiré pattern of straight equi-spaced fittings illustrates the interference fringes in plane *B* shown in Fig. 16.4b.

Superimposing two interferograms and looking at the moiré or beat produced can be extremely useful. The moiré formed by superimposing two different



Plane A —————



Plane B |

**Figure 16.4.** Interference of two spherical waves. (a) Circular line grating representing a spherical wavefront. (b) Moiré pattern obtained by superimposing two circular line patterns. (c) Fringes observed in plane A. (d) Fringes observed in plane B.



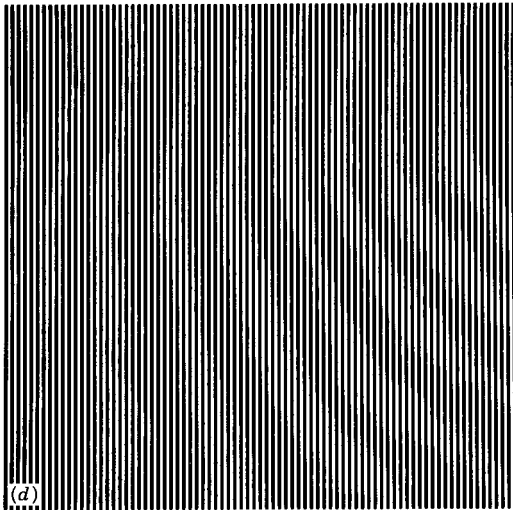
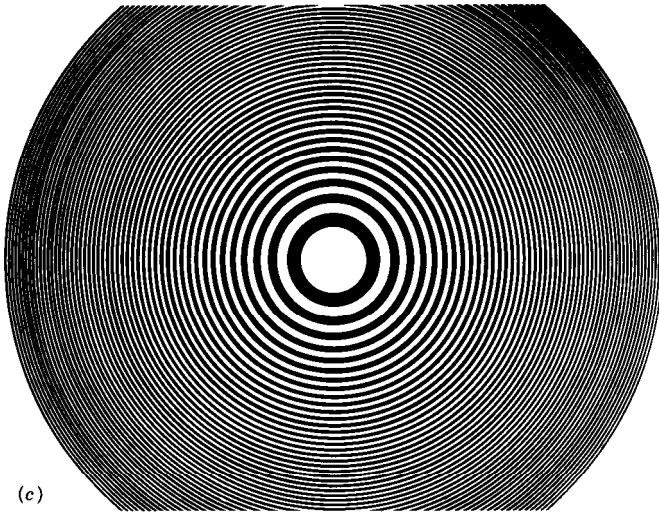
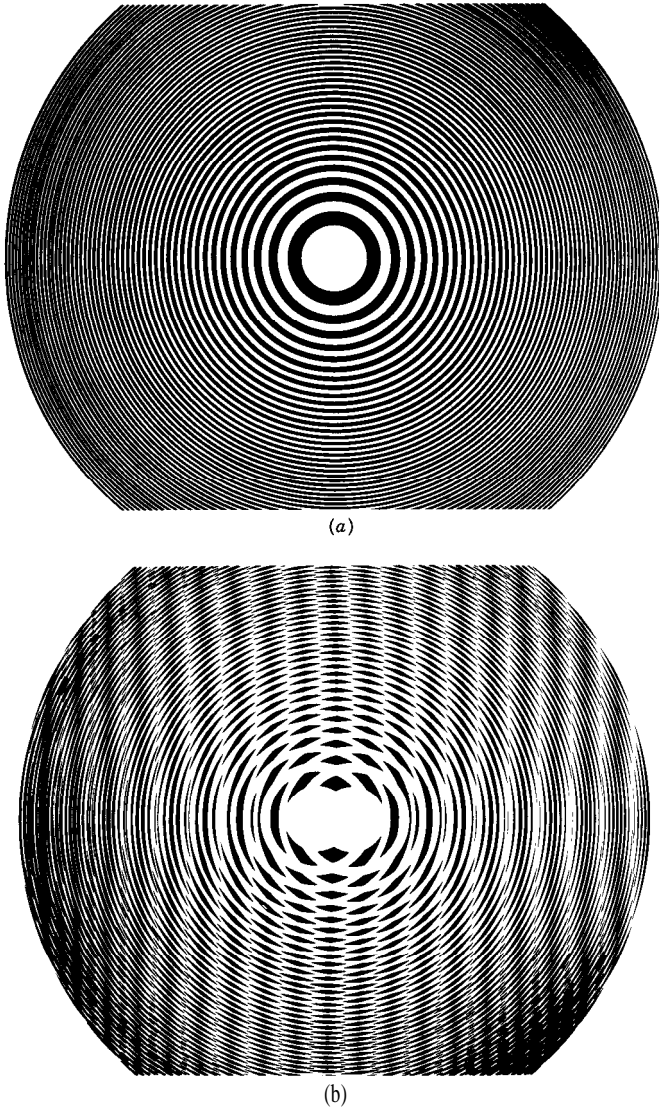


Figure 16.4. (Continued)

interferograms shows the difference in the aberrations of the two interferograms. For example, Fig. 16.6 shows the moiré produced by superimposing two computer-generated interferograms. One interferogram has 50 waves of tilt across the radius (Fig. 16.6a), while the second interferogram has 50 waves of tilt plus 4 waves of defocus (Fig. 16.6b). If the interferograms are aligned such that the tilt direction is the same for both interferograms, the tilt will cancel and



**Figure 16.5.** Moiré pattern produced by two zone plates. (a) Zone plate. (b) Straight-line fringes resulting from superposition of two zone plates.

only the 4 waves of defocus remain (Fig. 16.6c). In Fig. 16.6d, the two interferograms are rotated slightly with respect to each other so that the tilt will not quite cancel. These results can be described mathematically by looking at the two grating functions:

$$\phi_1(x, y) = 2\pi(50\rho \cos \phi + 4\rho^2)$$

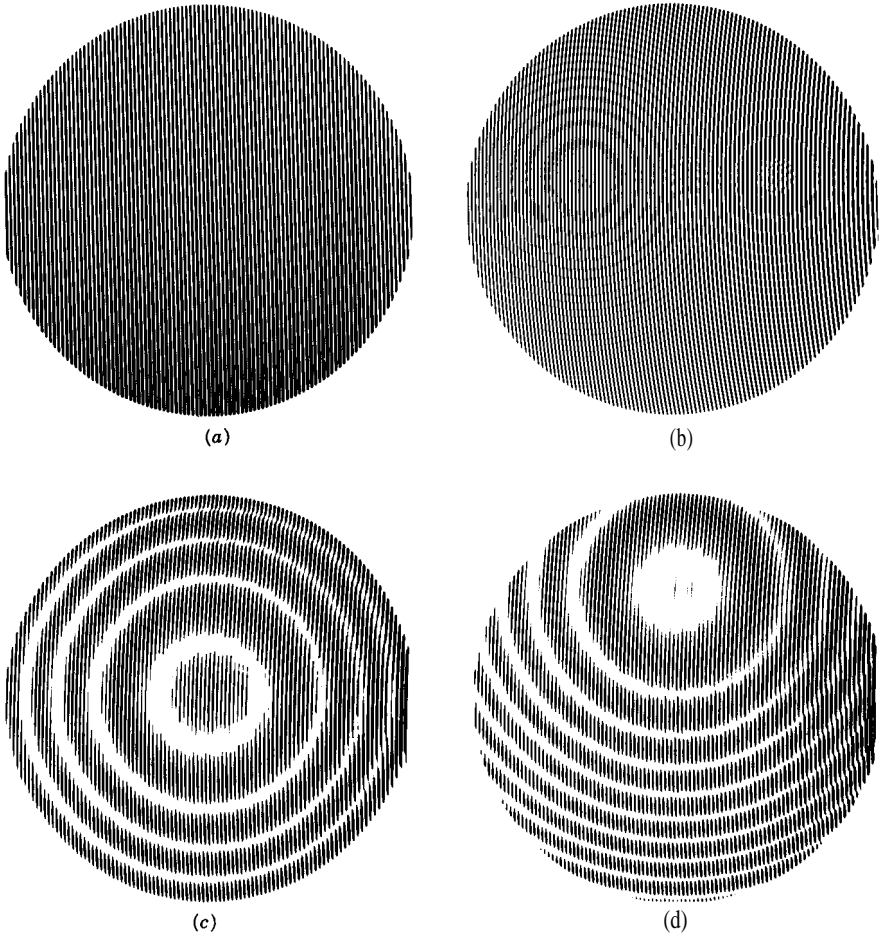


**Figure 16.6.** Moiré between two interferograms. (a) Interferogram having 50 waves tilt. (b) Interferogram having 50 waves tilt plus 4 waves of defocus. (c) Superposition of (a) and (b) with no tilt between patterns. (d) Slight tilt between patterns.

and

$$\phi_2(x, y) = 2\pi[50\rho \cos(\phi + \alpha)]. \quad (16.16)$$

A bright fringe is obtained when

$$50\rho[\cos\phi - \cos(\phi + \alpha)] + 4\rho^2 = M. \quad (16.17)$$

If  $\alpha = 0$ , the tilt cancels completely and four waves of defocus remain; otherwise, some tilt remains in the moiré pattern.

Figure 16.7 shows similar results for interferograms containing third-order aberrations. Spherical aberration with defocus and tilt is shown in Fig. 16.7d. One interferogram has 50 waves of tilt (Fig. 16.6a), and the other has 55 waves tilt, 6 waves third-order spherical aberration, and -3 waves defocus (Fig. 16.7a). Figure 16.7e shows the moiré between an interferogram having 50 waves of tilt (Fig. 16.6a) with an interferogram having 50 waves of tilt and 5 waves of coma (Fig. 16.7b) with a slight rotation between the two patterns. The moiré between an interferogram having 50 waves of tilt (Fig. 16.6a) and one having 50 waves of tilt, 7 waves third-order astigmatism, and -3.5 waves defocus (Fig. 16.7c) is shown in Fig. 16.7f. Thus, it is possible to produce simple fringe patterns using moiré. These patterns can be photocopied onto transparencies and used as a learning aid to understand interferograms obtained from third-order aberrations.

A computer-generated interferogram having 55 waves of tilt across the radius, 6 waves of spherical and -3 waves of defocus is shown in Fig. 16.7a. Figure 16.8a shows two identical interferograms superimposed with a small rotation between them. As expected, the moiré pattern consists of nearly straight equi-spaced lines. When one of the two interferograms is slipped over, the resultant moiré is shown in Fig. 16.8b. The fringe deviation from straightness in one interferogram is to the right and, in the other, to the left. Thus the sign of the defocus and spherical aberration for the two interferograms is opposite, and the moiré pattern has twice the defocus and spherical of each of the individual interferograms. When two identical interferograms given by Fig. 16.7a are superimposed with a displacement from one another, a shearing interferogram is obtained. Figure 16.9 shows vertical and horizontal displacements with and without a rotation between the two interferograms. The rotations indicate the addition of tilt to the interferograms. These types of moiré patterns are very useful for understanding lateral shearing interferograms.

Moiré patterns are produced by multiplying two intensity-distribution functions. **Adding two intensity functions does not give the difference term obtained in Eq. (16.3). A moiré pattern is not obtained if two intensity functions are added. The only way to get a moiré pattern by adding two intensity functions is to use a nonlinear detector.** For the detection of an intensity distribution given by  $I_1 + I_2$ , a nonlinear response can be written as

$$\text{Response} = a(I_1 + I_2) + b(I_1 + I_2)^2 + \dots \quad (16.18)$$

This produces terms proportional to the product of the two intensity distributions in the output signal. Hence, a moiré pattern is obtained if the two individual intensity patterns are simultaneously observed by a nonlinear detector (even if they are not multiplied before detection). If the detector produces an output linearly proportional to the incoming intensity distribution, the two intensity patterns must be multiplied to produce the moiré pattern. Since the eye

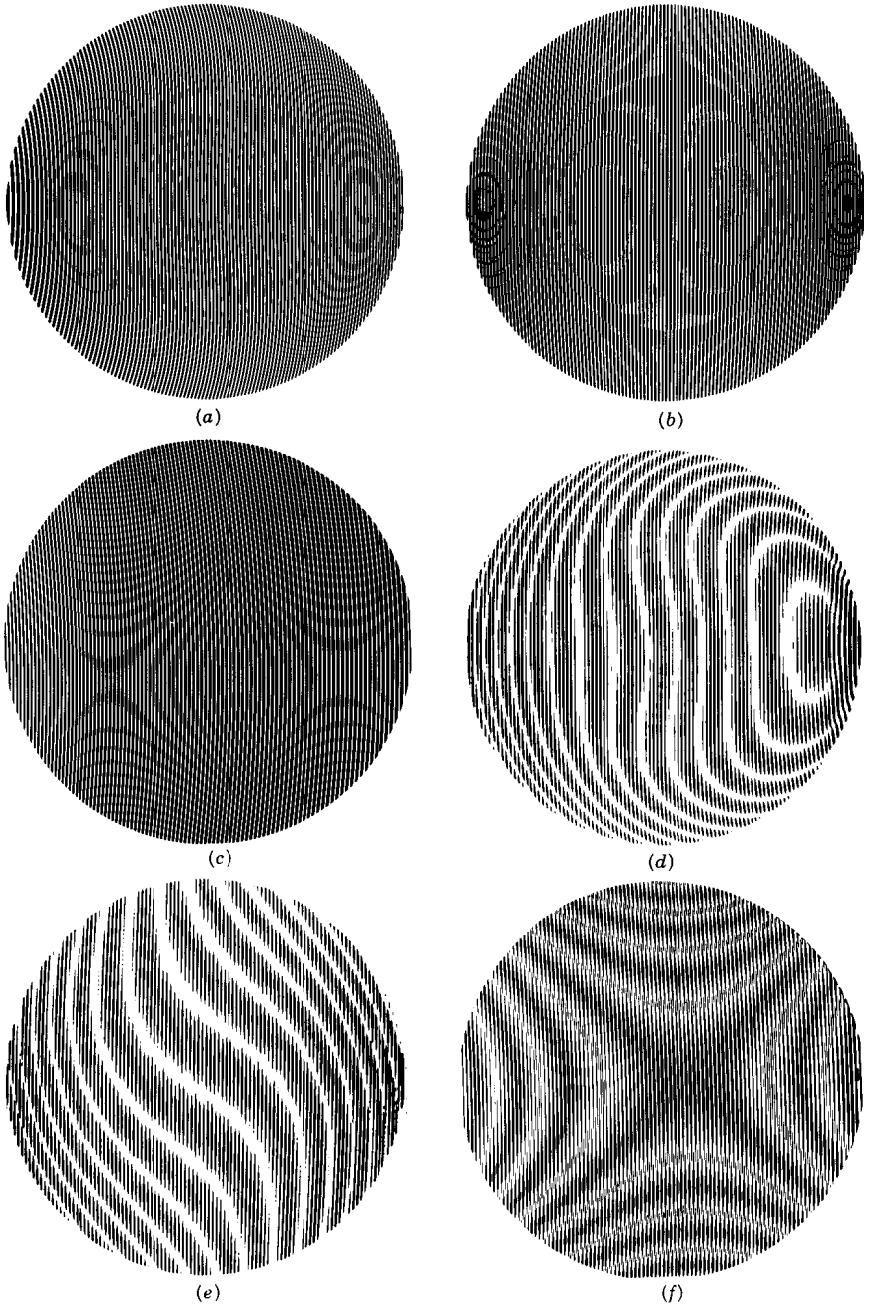


**Figure 16.7.** Moiré patterns showing third-order aberrations. Interferograms containing (a) 55 waves tilt, 6 waves of third-order spherical aberration, and  $-3$  waves of defocus, (b) 50 waves tilt and 5 waves coma, and (c) 50 waves tilt, 7 waves astigmatism, and  $-3.5$  waves of defocus. (d) Moiré pattern between Fig. 16.6a and 16.7a. (e) Moiré pattern between Fig. 16.6a and 16.7b. (f) Moiré pattern between Fig. 16.6a and 16.7c.

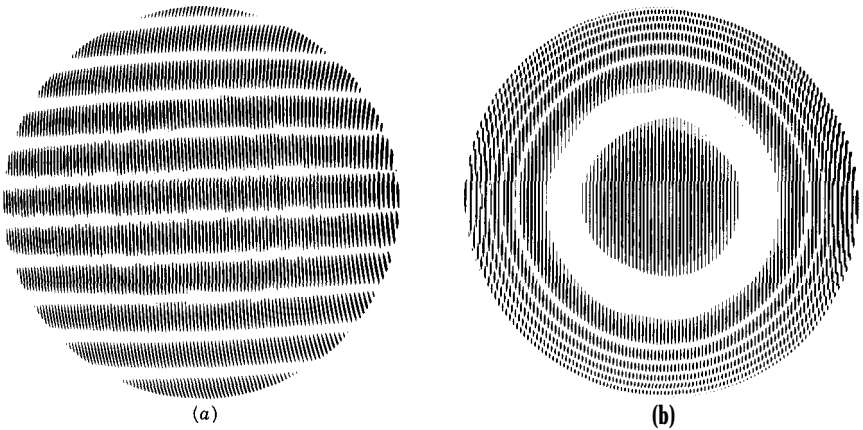


**Figure 16.8.** Moiré pattern by superimposing two identical interferograms (from Fig. 16.7a). (a) Both patterns having the same orientation. (b) With one pattern flipped.

is a nonlinear detector, moiré can be seen whether the patterns are added or multiplied. A good TV camera, on the other hand, will not see moiré unless the patterns are multiplied.

#### 16.4. HISTORICAL REVIEW

Since Lord Rayleigh first noticed the phenomena of moiré fringes, moiré techniques have been used for a number of testing applications. Righi (1887) first noticed that the relative displacement of two gratings could be determined by observing the movement of the moiré fringes. The next significant advance in the use of moiré was presented by Weller and Shepherd (1948). They used moiré to measure the deformation of an object under applied stress by looking at the differences in a grating pattern before and after the applied stress. They were the first to use shadow moiré, where a grating is placed in front of a nonflat surface to determine the shape of the object behind it by using the shape of the moiré fringes. A rigorous theory of moiré fringes did not exist until the mid-fifties when Ligtenberg (1955) and Guild (1956, 1960) explained moiré for stress analysis by mapping slope contours and displacement measurement, respectively. Excellent historical reviews of the early work in moiré have been presented by Theocaris (1962, 1966). Books on this subject have been written by Guild (1956, 1960), Theocaris (1969), and Durelli and Parks (1970). Projection moiré techniques were introduced by Brooks and Helfinger (1969) for optical gauging and deformation measurement. Until 1970, advances in moiré techniques were primarily in stress analysis. Some of the first uses of moiré to measure surface topography were reported by Meadows *et al.* (1970), Takasaki

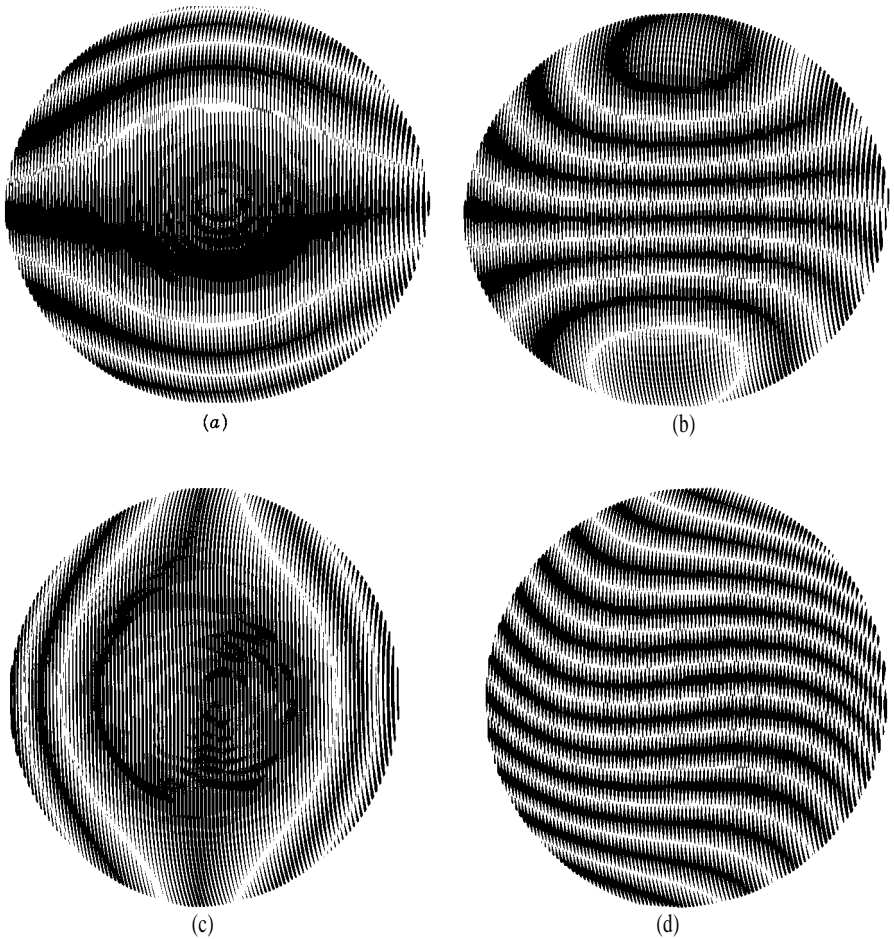


**Figure 16.9.** Moiré patterns formed using two identical interferograms (from Fig. 16.7a) where the two are sheared with respect to one another. (a) Vertical displacement. (b) Vertical displacement with rotation showing tilt. (c) Horizontal displacement. (d) Horizontal displacement with rotation showing tilt.

(1970), and Wasowski (1970). Moiré has also been used to compare an object to a master and for vibration analysis (Der Hovanesian and Yung 1971; Gasvik 1987). A theoretical review and experimental comparison of moiré and projection techniques for contouring is given by Benoit et al. (1975). Automatic computer fringe analysis of moiré patterns by finding fringe centers were reported by Yatagai et al. (1982). Heterodyne interferometry was first used with moiré fringes by Moore and Truax (1977), and phase measurement techniques were further developed by Perrin and Thomas (1979), Shagam (1980), and Reid

(1984b). Recent review papers on moiré techniques include Post (1982), Reid (1984a), and Halioua and Liu (1989).

The projection of interference fringes for contouring objects was first proposed by Rowe and Welford (1967). Their later work included a number of applications for projected fringes (Welford 1969) and the use of projected fringes with holography (Rowe 1971). In-depth mathematical treatments have been provided by Benoit et al. (1975) and Gasvik (1987). The relationship between projected fringe contouring and triangulation is given in a book chapter by Case et al. (1987). Heterodyne phase measurement was first introduced with projected fringes by Indebetouw (1978), and phase measurement techniques were further developed by Takeda et al. (1982), Takeda and Mutoh (1983), and Srinivasan et al. (1984, 1985).

Haines and Hildebrand first proposed contouring objects in holography using two sources (Haines and Hildebrand 1965; Hildebrand and Haines 1966, 1967). The two holographic sources were produced by changing either the angle of the illumination beam on the object or the angle of the reference beam. A small angle difference between the beams used to produce a double-exposure hologram creates a moiré in the final hologram which corresponds to topographic contours of the test object. Further insight into two-angle holography has been provided by Menzel (1974), Abramson (1976a, 1976b) and DeMattia and Fos-sati-Bellani (1978). The technique has also been used in speckle interferometry (Winther, 1983).

Since all of these techniques are so similar, it is sometimes hard to differentiate developments in one technique versus another. MacGovern (1972) provided a theory that linked all of these techniques together. The next part of this chapter will explain each of these techniques and then show the similarities among all of these techniques and provide a comparison to conventional interferometry.

## 16.5. FRINGE PROJECTION

A simple approach for contouring is to project interference fringes or a grating onto an object and then view from another direction. Figure 16.10 shows the

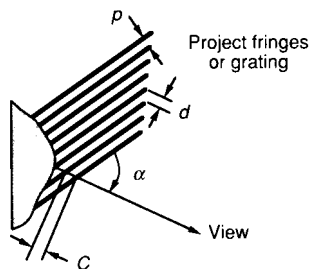


**Figure 16.10.** Projection of fringes or grating onto object and viewed at an angle  $\alpha$ .  $p$  is the grating pitch or fringe spacing and  $C$  is the contour interval.



optical setup for this measurement. Assuming a collimated illumination beam and viewing the fringes with a telecentric optical system, straight equally spaced fringes are incident on the object, producing equally spaced contour intervals. The departure of a viewed fringe from a straight line shows the departure of the surface from a plane reference surface. An object with fringes projected onto it can be seen in Fig. 16.11. When the fringes are viewed at an angle  $\alpha$  relative

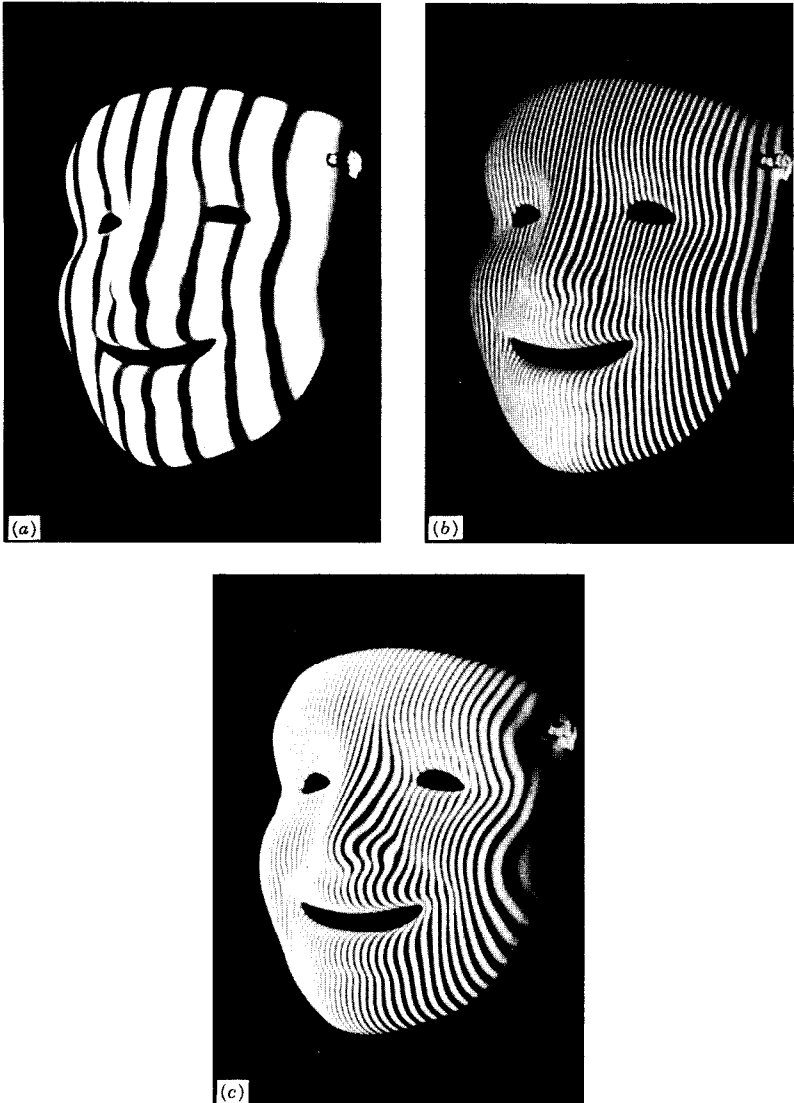


**Figure 16.11.** Mask with fringes projected onto it. (a) Coarse fringe spacing. (b) Fine fringe spacing. (c) Fine fringe spacing with an increase in the angle between illumination and viewing.

to the projection direction, the spacing of the lines perpendicular to the viewing direction will be

$$d = \frac{P}{\cos \alpha}. \quad (16.19)$$

The contour interval  $C$  (the height between adjacent contour lines in the viewing direction) is determined by the line or fringe spacing projected onto the surface and the angle between the projection and viewing directions;

$$C = \frac{p}{\sin \alpha} = \frac{d}{\tan \alpha}. \quad (16.20)$$

These contour lines are planes of equal height, and the sensitivity of the measurement is determined by  $\alpha$ . The larger the angle  $\alpha$ , the smaller the contour interval. If  $\alpha = 90^\circ$ , then the contour interval is equal top, and the sensitivity is a maximum. The reference plane will be parallel to the direction of the fringes and perpendicular to the viewing direction as shown in Fig. 16.12. Even though the maximum sensitivity can be obtained at  $90^\circ$ , this angle between the projection and viewing directions will produce a lot of unacceptable shadows on the object. These shadows will lead to areas with missing data where the object cannot be contoured. When  $\alpha = 0$ , the contour interval is infinite, and the measurement sensitivity is zero. To provide the best results, an angle no larger than the largest slope on the surface should be chosen.

When interference fringes are projected onto a surface rather than using a grating, the fringe spacing  $p$  is determined by the geometry shown in Fig. 16.13

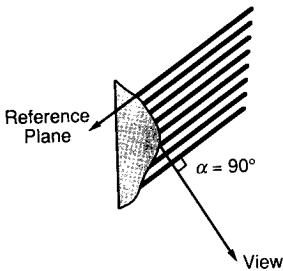


**Figure 16.12.** Maximum sensitivity for fringe projection with a  $90^\circ$  angle between projection and viewing.

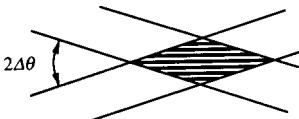


**Figure 16.13.** Fringes produced by two interfering beams.

and is given by

$$p = \frac{\lambda}{2 \sin \Delta\theta}, \quad (16.21)$$

where  $\lambda$  is the wavelength of illumination and  $2\Delta\theta$  is the angle between the two interfering beams. Substituting the expression for  $p$  into Eq. (16.20), the contour interval becomes

$$C = \frac{\lambda}{2 (\sin \Delta\theta) \sin \alpha}. \quad (16.22)$$

If a simple interferometer such as a Twyman-Green is used to generate projected interference fringes, tilting one beam with respect to the other will change the contour interval. The larger the angle between the two beams, the smaller the contour interval will be. Figures 16.11a and 16.11b show a change in the fringe spacing for interference fringes projected onto an object. The direction of illumination has been moved away from the viewing direction between Figs. 16.11b and 16.11c. This increases the angle  $\alpha$  and the test sensitivity while reducing the contour interval. Projected fringe contouring has been covered in detail by Gasvik (1987).

If the source and the viewer are not at infinity, the fringes or grating projected onto the object will not be composed of straight, equally spaced lines. The height between contour planes will be a function of the distance from the source and viewer to the object. There will be a distortion due to the viewing of the fringes as well as due to the illumination. This means that the reference surface will not be a plane. As long as the object does not have large height changes compared to the illumination and viewing distances, a plane reference surface placed in the plane of the object can be measured first and then subtracted from subsequent measurements of the object. This enables the mapping of a plane in object space to a surface that will serve as a reference surface. If the object has large height variations, the plane reference surface may have to be measured in a number of planes to map the measured object contours to real heights. Finite illumination and viewing distances will be considered in more detail with shadow moiré in the next section.

## 16.6 SHADOW MOIRÉ

A simple method of moiré interferometry for contouring objects uses a single grating placed in front of the object as shown in Fig. 16.14. The grating in front of the object produces a shadow on the object that is viewed from a different direction through the grating. A low-frequency beat or moiré pattern is seen.

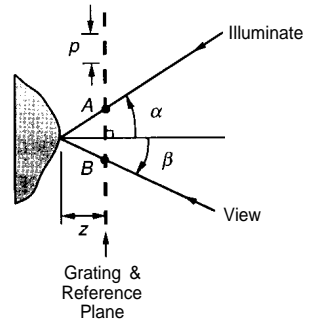


**Figure 16.14.** Geometry for shadow moiré with illumination and viewing at infinity, i.e., parallel illumination and viewing.

This pattern is due to the interference between the grating shadows on the object and the grating as viewed. Assuming that the illumination is collimated and that the object is viewed at infinity or through a telecentric optical system, the height  $z$  between the grating and the object point can be determined from the geometry shown in Fig. 16.14 (Meadows et al. 1970; Takasaki 1973; Chiang 1983). This height is given by

$$z = \frac{Np}{\tan \alpha + \tan \beta}, \quad (16.23)$$

where  $\alpha$  is the illumination angle,  $\beta$  is the viewing angle,  $p$  is the spacing of the grating lines, and  $N$  is the number of grating lines between the points  $A$  and  $B$  (see Fig. 16.14). The contour interval in a direction perpendicular to the grating will simply be given by

$$C = \frac{p}{\tan \alpha + \tan \beta}. \quad (16.24)$$

Again, the distance between the moiré fringes in the beat pattern depends on the angle between the illumination and viewing directions. The larger the angle, the smaller the contour interval. If the high frequencies due to the original grating are filtered out, then only the moiré interference term is seen. The reference plane will be parallel to the grating. Note that this reference plane is tilted with respect to the reference plane obtained when fringes are projected onto the subject. Essentially, the shadow moiré technique provides a way of removing the "tilt" term and repositioning the reference plane. The contour interval for shadow moiré is the same as that calculated for projected fringe contouring (Eq. (16.20)) when one of the angles is zero with  $d = p$ . Figure 16.15 shows an object that has a grating sitting in front of it. An illumination beam is projected from one direction and viewed from another direction. Between Figs. 16.5a and 16.5b, the angles  $\alpha$  and  $\beta$  have been increased. This has the effect of

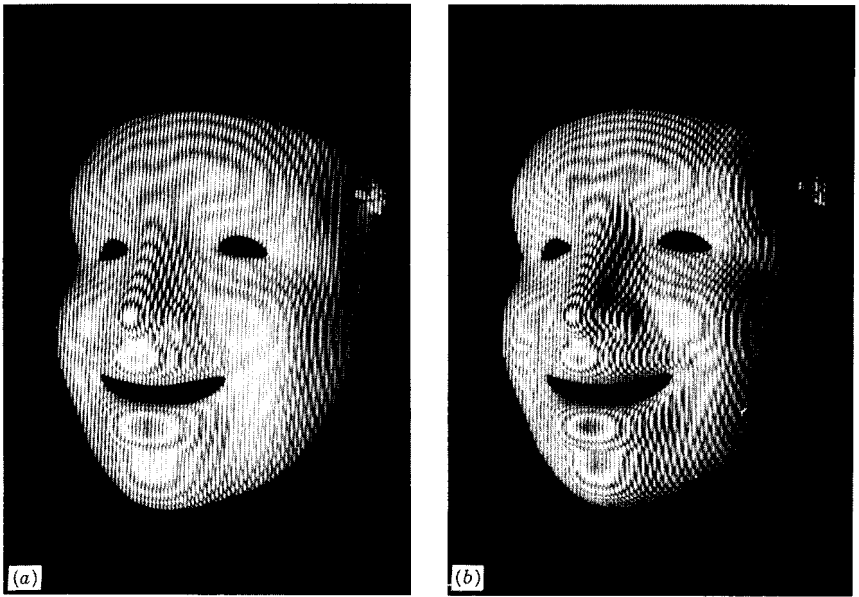


**Figure 16.15.** Mask with grating in front of it. (a) One viewing angle. (b) Larger viewing angle.

decreasing the contour interval, increasing the number of fringes, and rotating the reference plane slightly away from the viewer.

Most of the time, it is difficult to illuminate an entire object with a collimated beam. Therefore, it is important to consider the case of finite illumination and viewing distances. It is possible to derive this for a very general case (Meadows et al. 1970; Takasaki 1970; Bell 1985); however, for simplicity, only the case where the illumination and viewing positions are the same distance from the grating will be considered. Figure 16.16 shows a geometry where the distance between the illumination source and the viewing camera is given by  $w$ , and the distance between these and the grating is  $l$ . The grating is assumed to be close enough to the object surface so that diffraction effects are negligible. In this

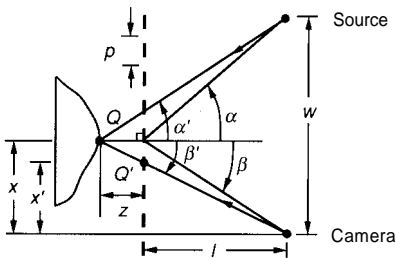


**Figure 16.16.** Geometry for shadow moiré with illumination and viewing at finite distances.

case the height between the object and the grating is given by

$$z = \frac{Np}{\tan \alpha' + \tan \beta'}, \quad (16.25)$$

where  $\alpha'$  and  $\beta'$  are the illumination and viewing angles at the object surface. These angles change for every point on the surface and are different from  $\alpha$  and  $\beta$  in Fig. 16.16, where  $\alpha$  and  $\beta$  are the illumination and viewing angles at the grating (reference) surface. The surface height can also be written as (Meadows et al. 1970; Takasaki 1973; Chiang 1983)

$$z = NC(z) = \frac{Np(l + z)}{w} = \frac{Npl}{w - Np}. \quad (16.26)$$

This equation indicates that the height is a complex function depending on the position of each object point. Thus, the distance between contour intervals is dependent on the height of the surface and the number of fringes between the grating and the object. Individual contour lines will no longer be planes of equal height. They are now surfaces of equal height. The expression for height can be simplified by considering the case where the distance to the source and viewer is large compared to the surface height variations,  $l \gg z$ . Then the surface height can be expressed as

$$z = \frac{Npl}{w} = \frac{Np}{\tan \alpha + \tan \beta}. \quad (16.27)$$

Even though the angles  $\alpha$  and  $\beta$  vary from point-to-point on the surface, the sum of their tangents remains equal to  $w/l$  for all object points as long as  $l \gg z$ . The contour interval will be constant in this regime and will be the same as that given by Eq. (16.24).

Because of the finite distances, there is also distortion due to the viewing perspective. A point on the surface  $Q$  will appear to be at the location  $Q'$  when viewed through the grating. By similar triangles, the distances  $x$  and  $x'$  from a line perpendicular to the grating intersecting the camera location can be related using

$$\frac{x}{z + l} = \frac{x'}{l}, \quad (16.28)$$

where  $x$  and  $x'$  are defined in Fig. 16.16. Equation (16.28) can be rearranged to yield the actual coordinate  $x$  in terms of the measured coordinate  $x'$  and the measurement geometry,

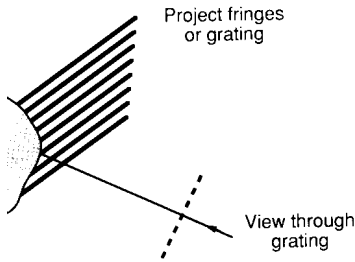


**Figure 16.17.** Projection moiré where fringes or a grating are projected onto a surface and viewed through a second grating.

$$x = x' \left( 1 + \frac{z}{l} \right). \quad (16.29)$$

Likewise, the  $y$  coordinate can be corrected using

$$y = y' \left( 1 + \frac{z}{l} \right). \quad (16.30)$$

This enables the measured surface to be mapped to the actual surface to correct for the viewing perspective. These same correction factors can be applied to fringe projection.

## 16.7. PROJECTION MOIRÉ

Moiré interferometry can also be implemented by projecting interference fringes or a grating onto an object and then viewing through a second grating in front of the viewer (see Fig. 16.17) (Brooks and Helfinger 1969). The difference between projection and shadow moiré is that two different gratings are used in projection moiré. The orientation of the reference plane can be arbitrarily changed by using different grating pitches to view the object. The contour interval is again given by Eq. (16.24), where  $d$  is the period of the grating in the  $y$  plane, as long as the grating pitches are matched to have the same value of  $d$ . This implementation makes projection moiré the same as shadow moiré, although projection moiré can be much more complicated than shadow moiré. A good theoretical treatment of projection moiré is given by Benoit et al. (1975).

## 16.8. TWO-ANGLE HOLOGRAPHY

Projected fringe contouring can also be done using holography. First a hologram of the object is made using the optical setup shown in Fig. 16.18. Then the direction of the beam illuminating the object is changed slightly. When the

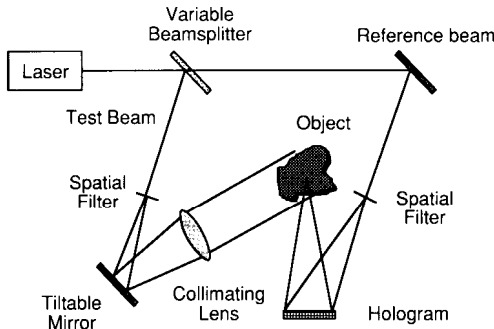


Figure 16.18. Setup for two-angle holographic interferometry

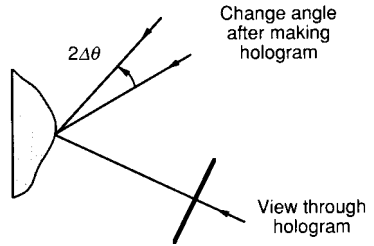


Figure 16.19. Two-angle holographic interferometric. Interference fringes resulting from shifting the illumination beam.

object is viewed through the hologram, interference fringes are seen that correspond to the interference between the wavefront stored in the hologram and the live wavefront with the tilted illumination. This process is depicted by Fig. 16.19. These fringes are exactly what would be seen if the object were illuminated with the two illumination beams simultaneously. The beams would be tilted with respect to one another by the same amount that the illumination beam was tilted after making the hologram. These fringes will look the same as those produced by projected fringe contouring and shown in Fig. 16.11. To produce straight, equally spaced fringes, the object illumination should be collimated. When collimated illumination is used, the surface contour is measured relative to a surface that is a plane. The theory of projected fringe contouring can be applied to two-angle holographic contouring yielding a contour interval given by Eq. (16.22), where  $2\Delta\theta$  is the change in the angle of the object illumination. More detail on two-angle holographic contouring can be found in Haines and Hildebrand (1965), Hildebrand and Haines (1966, 1967), Vest (1979), and Harriharan (1984).

### 16.9. COMMON FEATURES

All of the techniques described produce fringes corresponding to contours of equal height on the object. They all have a similar contour interval determined



by the fringe spacing or grating period and the angle between the illumination and viewing directions as long as the illumination and viewing are collimated. Phase shifting can be applied to any of the techniques to produce quantitative height information as long as sinusoidal fringes are present at the camera. The surface heights measured are relative to a reference surface that is a plane as long as the fringes or grating lines are straight and equally spaced at the object. The only difference between the moiré techniques and the projected fringes and two-angle holography is the change in the location of the reference plane. If the fringes are digitized or phase-measuring interferometry techniques are applied, the reference plane can be changed in the computer mathematically.

The precision of these contouring techniques depends on the number of fringes used. When the fringes are digitized using fringe-following techniques, the surface height can be determined to 1/10 of a fringe. If phase measurement is used, the surface heights can be determined to 1/100 of a fringe. Therefore it is advantageous to use as many fringes as possible. And because a reference plane can easily be changed in a computer, projected fringe contouring is the simplest way to contour an object interferometrically.

## 16.10. COMPARISON TO CONVENTIONAL INTERFEROMETRY

The measurement of surface contour can be related to making the same measurement using a Twyman-Green interferometer assuming a long effective wavelength. The loci of the lines or fringes projected onto the surface (assuming illumination and viewing at infinity) is given by

$$y = z \tan \alpha + nd, \quad (16.31)$$

where  $z$  is the height of the surface at the point  $y$ ,  $d$  is the fringe spacing measured along the  $y$  axis, and  $n$  is an integer referring to fringe order number. If the same surface were tested using a Twyman-Green interferometer, a bright fringe would be obtained whenever

$$2z - y \sin \gamma = n\lambda, \quad (16.32)$$

where  $\lambda$  is the wavelength and  $\gamma$  is the tilt of the reference plane. By comparing Eqs. (16.31) and (16.32), it can be seen that they are equivalent as long as

$$d = \frac{\lambda_{\text{effective}}}{\sin \gamma} \quad (16.33)$$

and

$$\frac{2}{\sin \gamma} = \tan \alpha, \quad (16.34)$$

where  $\lambda_{\text{effective}}$  is the effective wavelength. The effective wavelength can then be written as

$$\lambda_{\text{effective}} = 2C = \frac{2d}{\tan \alpha} = \frac{2p}{\cos \alpha \tan \alpha}, \quad (16.35)$$

where  $C$  is the contour interval as defined in Eq. (16.20). Thus, contouring using these techniques is similar to measuring the object in a Twyman-Green interferometer using a source with wavelength  $\lambda_{\text{effective}}$ .

### 16.11. APPLICATIONS

These techniques can all be used for displacement measurement or stress analysis as well as for contouring objects. Displacement measurement is performed by comparing the fringe patterns obtained before and after a small movement of the object or before and after applying a load to the object. Because the sensitivity of these tests are variable, they can be used for a larger range of displacements and stresses than the holographic techniques. Differential interferometry comparing two objects or an object and a master can also be performed by comparing the two fringe patterns obtained. Finally, time-average vibration analysis can also be performed with moiré, yielding results similar to those obtained with time-average holography with a much longer effective wavelength.

Using phase-measurement techniques, the surface height relative to some reference surface can be obtained quantitatively. If the contour lines are straight and equally spaced in object space, then the reference surface will be a plane. In the computer, any plane (or surface) desired can be subtracted from the surface height to yield the surface profile relative to any plane (or surface). This is similar to viewing the contour lines through a grating (or deformed grating) to reduce their number. If the contour lines are not straight and equally spaced, the reference surface will be something other than a plane. The reference surface can be determined by placing a flat surface at the location of the object and measuring the surface height. Once this reference surface is measured, it can be subtracted from subsequent measurements to yield the surface height relative to a plane surface. Thus, with the use of phase-measuring interferometry techniques, the surface height can be made relative to any surface and transformed to surface heights relative to another surface. Taking this one step further, a master component can be compared to a number of test components to determine if their shape is within the specification. It should also be pointed out that this measurement is sensitive to a certain direction, and that there may be areas where data are missing because of shadows on the surface.

As an example, Fig. 16.20 shows the mask of Figs. 16.11 and 16.15 con-

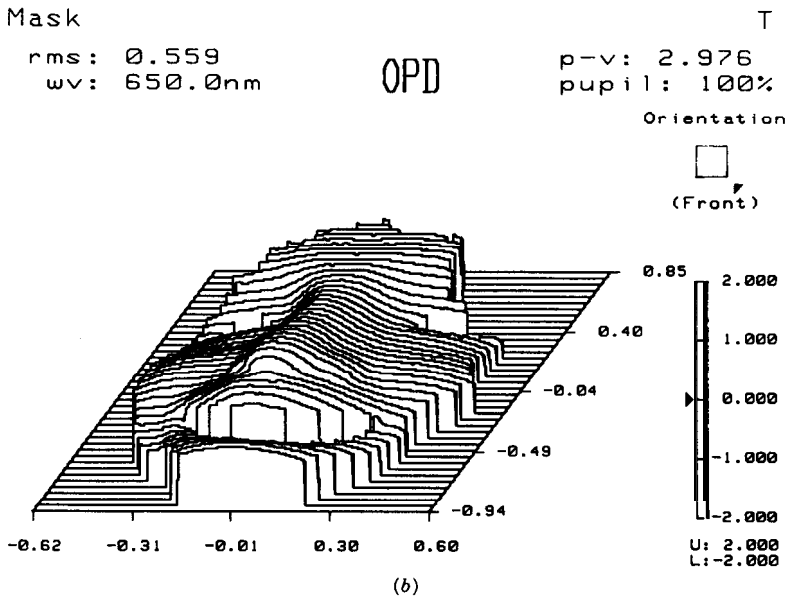
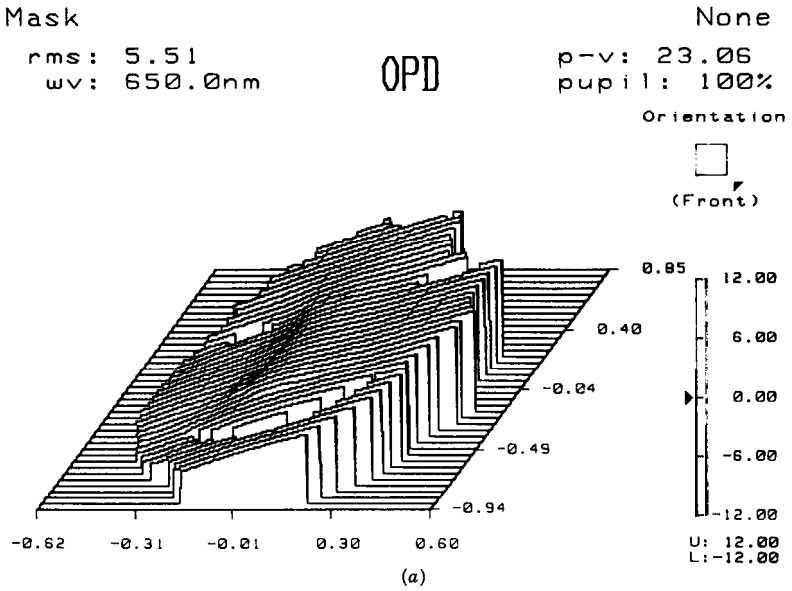


**Figure 16.20.** Mask measured with projected fringes and phase-measurement interferometry. (a) Isometric plot of measured surface height. (b) Isometric plot after best-fit plane removed. (c) Two-dimensional contour plot of measured surface height. (d) Two-dimensional contour plot after best-fit plane removed. Units on plots are in number of contour intervals. One contour interval is approximately 10 mm. The surface is about 150 mm in diameter.

Mask None  
 rms: 5.51 Interval: 2.000 p-v: 23.06  
 wv: 650.0nm pupil: 100%



(c)

Mask T  
 rms: 0.559 Interval: 0.500 p-v: 2.976  
 wv: 650.0nm pupil: 100%



(d)

Figure 16.20. (Continued)

toured using fringe projection and phase-measurement interferometry. The fringes are produced using a Twyman-Green interferometer with a He-Ne laser. A high-resolution camera with 1320 x 900 pixels and a zoom lens is used to view the fringes. Surface heights are calculated using phase-measurement techniques at each detector point. A total of five interferograms were used to calculate the surface shown in Fig. 16.20a. The best-fit plane has been subtracted from the surface to yield Fig. 16.20b. In this way the reference plane has been changed. Figures 16.20c and 16.20d show two-dimensional contour maps of the object before and after the best-fit plane is removed. These contours can also be thought of as the fringes that would be viewed on the object. Figure 16.20c shows the fringes without a second grating, and Fig. 16.20d is with a

second reference grating chosen to minimize the fringe spacing. The contour interval for this example is 10 mm, and the total peak-to-valley height deviation after the tilt is subtracted is about 30 mm.

## 16.12. SUMMARY

The techniques of projected fringe contouring, projection moiré, shadow moiré, and two-angle holographic contouring are all similar. They all involve projecting a pattern of lines or interference fringes onto an object and then viewing those contour lines from a different direction. In the case of the moiré techniques, the contour lines are viewed through a grating to reduce the total number of fringes. In all of the techniques, the surface height is measured relative to a reference surface. The reference surface will be a plane if the projected grating lines or interference fringes are straight and equally spaced at the object and viewed at infinity or with a telecentric imaging system. The use of the second grating in the moiré techniques changes the reference plane but does not affect the contour interval. The sensitivity of the techniques is a maximum when the contour lines are viewed at an angle of  $90^\circ$  with respect to the projection direction. Quantitative data can be obtained from any of these techniques using phase-measurement interferometry techniques. The precision of the surface-height measurement will depend on the number of fringes present. Surface-height measurements can be made with a repeatability of 1/100 of a contour interval rms (root-mean-square). Thus, the number of fringes used should be as many as can easily be measured by the detection system. The contour interval can be changed to increase the number of fringes, and once the surface height is calculated, a reference surface can be subtracted in the computer to find the surface height relative to any desired surface.

**Acknowledgments.** The authors acknowledge the support of WYKO Corporation during the preparation of this manuscript.

## REFERENCES

- Abramson, N., "Sandwich Hologram Interferometry. 3: Contouring," *Appl. Opt.*, 15(1), 200-205 (1976a).
- Abramson, N., "Holographic Contouring by Translation," *Appl. Opt.*, 15(4), 1018-1022 (1976b).
- Bell, B., "Digital Heterodyne Topography," Ph.D. Dissertation, Optical Sciences Center, University of Arizona, Tucson, AZ, 1985.

- Benoit, P., E. Mathieu, J. Hormier, and A. Thomas, "Characterization and Control of Three Dimensional Objects Using Fringe Projection Techniques," *Nouv. Rev. Opt.*, **6(2)**, 67-86 (1975).
- Brooks, R. E. and L. O. Heflinger, "Moiré Gauging Using Optical Interference Patterns," *Appl. Opt.*, 8(5), 935-939 (1969).
- Case, S. K., J. A. Jalkio, and R. C. Kim, "3-D Vision System Analysis and Design," in *Three-Dimensional Machine Vision*, Takeo Kanade, Ed., Kluwer Academic Publishers, Norwell, MA, 1987, pp. 63-95.
- Chiang, F.-P., "Moiré Methods for Contouring, Displacement, Deflection, Slope and Curvature," *Proc. SPIE*, **153**, 113-119 (1978).
- Chiang, F.-P., "Moiré Methods of Strain Analysis," in *Manual on Experimental Stress Analysis*, A. S. Kobayashi, Ed., Soc. for Exp. Stress Anal., Brookfield Center, CT, 1983, pp. 51-69.
- DeMattia, P. and V. Fossati-Bellani, "Holographic Contouring by Displacing the Object and the Illumination Beam," *Opt. Commun.*, 26(1), 17-21 (1978).
- Der Hovanesian, J. and Y. Y. Yung, "Moiré Contour-Sum Contour-Difference, and Vibration Analysis of Arbitrary Objects," *Appl. Opt.*, 10(12), 2734-2738 (1971).
- Dureli, A. J. and V. J. Parks, *Moiré Analysis of Strain*, Prentice-Hall, Englewood Cliffs, NJ, 1970.
- Gasvik, K. J., *Optical Metrology*, Wiley, Chichester, 1987.
- Guild, J., *The Interference Systems of Crossed Diffraction Gratings*, Clarendon Press, Oxford, 1956.
- Guild, J., *Diffraction Gratings as Measuring Scales*, Oxford University Press, London, 1960.
- Haines, K. and B. P. Hildebrand, "Contour Generation by Wavefront Reconstruction," *Phys. Lett.*, 19(1), 10-11 (1965).
- Halioua, M. and H.-C. Liu, "Optical Three-Dimensional Sensing by Phase Measuring Profilometry," *Opt. Lasers Eng.*, **11(3)**, 185-215 (1989).
- Hariharan, P., *Optical Holography*, Cambridge University Press, Cambridge, 1984.
- Hildebrand, B. P. and K. A. Haines, "The Generation of Three-Dimensional Contour Maps by Wavefront Reconstruction," *Phys. Lett.*, **21(4)**, 422-423 (1966).
- Hildebrand, B. P. and K. A. Haines, "Multiple-Wavelength and Multiple-Source Holography Applied to Contour Generation," *J. Opt. Soc. Am.*, 57(2), 155-162 (1967).
- Indebetouw, G., "Profile Measurement Using Projection of Running Fringes," *Appl. Opt.*, **17(18)**, 2930-2933 (1978).
- Ligtenberg, F. K., "The Moiré Method," *Proc. Soc. Exp. Stress Anal. (SESA)*, **12(2)**, 83-98 (1955).
- MacGover, A. J., "Projected Fringes and Holography," *Appl. Opt.*, **11(12)**, 2972-2974 (1972).
- Meadows, D. M., W. O. Johnson, and J. B. Allen, "Generation of Surface Contours by Moiré Patterns," *Appl. Opt.*, 9(4), 942-947 (1970).
- Menzel, E., "Comment to the Methods of Contour Holography," *Optik*, 40(5), 557-559 (1974).

- Moore, D. T. and B. E. Truax, "Phase-Locked Moiré Fringe Analysis for Automated Contouring of Diffuse Surfaces," *Appl. Opt.*, 18(1), 91-96 (1979).
- Oster, G. and Y. Nishijima, "Moiré Patterns," *Sci. Amer.*, 208(5), 54-63 (May 1963).
- Perrin, J. C. and A. Thomas, "Electronic Processing of Moiré Fringes: Application to Moiré Topography and Comparison with Photogrammetry," *Appl. Opt.*, 18(4), 563-574 (1979).
- Post, D., "Developments in Moiré Interferometry," *Opt. Eng.*, 21(3), 458-467 (1982).
- Rayleigh, Lord, "On the Manufacture and Theory of Diffraction-Gratings," *Phil. Mag.* S.4, 47(310) 81-93 and 193-205 (1874).
- Reid, G. T., "Moiré Fringes in Metrology," *Opt. Lasers Eng.*, 5(2), 63-93 (1984a).
- Reid, G. T., R. C. Rixon, and H. I. Messer, "Absolute and Comparative Measurements of Three-Dimensional Shape by Pulse Measuring Moiré Topography," *Opt. Laser Tech.*, 16(6), 315-319 (1984b).
- Righi, A., "Sui Fenomeni Che si Producono colla Sovrapposizione dei Due Reticoli e sopra Alcune Lora Applicazioni: I," *Nuovo Cim.*, 21, 203-227 (1887).
- Rowe, S. H., "Projected Interference Fringes in Holographic Interferometry," *J. Opt. Soc. Am.*, 61(12), 1599-1603 (1971).
- Rowe, S. H. and W. T. Welford, "Surface Topography of Non-Optical Surfaces by Projected Interference Fringes," *Nature*, 216(5117), 786-787 (1967).
- Shagam, R., "Heterodyne Interferometric Method for Profiling Recorded Moiré Interferograms," *Opt. Eng.*, 19(6), 806-809 (1980).
- Srinivasan, V., H. C. Liu, and M. Halioua, "Automated Phase-Measuring Profilometry of 3-D Diffuse Objects," *Appl. Opt.*, 23(18), 3015-3108 (1984).
- Srinivasan, V., H. C. Liu, and M. Halioua, "Automated Phase-Measuring Profilometry: A Phase Mapping Approach," *Appl. Opt.*, 24(2), 185-188 (1985).
- Takasaki, H., "Moiré Topography," *Appl. Opt.*, 9(6), 1467-1472 (1970).
- Takasaki, H., "Moiré Topography," *Appl. Opt.*, 12(4), 845-850 (1973).
- Takeda, M. and K. Mutoh, "Fourier Transform Profilometry for the Automatic Measurement of 3-D Object Shapes," *Appl. Opt.*, 22(24), 3977-3982 (1983).
- Takeda, M., H. Ina, and S. Kabayashi, "Fourier-Transform Method of Fringe-Pattern Analysis for Computer-Based Topography and Interferometry," *J. Opt. Soc. Am.*, 72(1), 156-160 (1982).
- Theocaris, P. S., "Moiré Fringes: A Powerful Measuring Device," *Appl. Mech. Rev.*, 15(5), 333-339 (1962).
- Theocaris, P. S., "Moiré Fringes: A Powerful Measuring Device," in *Applied Mechanics Surveys*, Spartan Books, Washington, D.C., 1966, p. 613-626.
- Theocaris, P. S., *Moiré Fringes in Strain Analysis*, Pergamon Press, Oxford, 1969.
- Vamer, J. R., "Holographic and Moiré Surface Contouring," in *Holographic Nondestructive Testing*, R. K. Erf, Ed., Academic Press, Orlando, 1974.
- Vest, C. M., *Holographic Interferometry*, Wiley, New York, 1979.
- Wasowski, J., "Moiré Topographic Maps," *Opt. Commun.*, 2(7), 321-323 (1970).
- Webster's Third New International Dictionary*, Merriam-Webster, Springfield, MA, 1981.

- Welford, W. T., "Some Applications of Projected Interference Fringes," *Opt. Acta*, **16(3)**, 371-376 (1969).
- Weller, R. and B. M. Shepherd, "Displacement Measurement by Mechanical Interferometry," *Proc. Soc. Exp. Stress Anal. (SESA)*, 6(1), 35-38 (1948).
- Winther, S. and G. A. Slettemoen, "An ESPI Contouring Technique in Strain Analysis," *Proc. SPIE*, **473**, 44-47 (1983).
- Yatagai, T., M. Idesawa, Y. Yamaashi, and M. Suzuki, "Interactive Fringe Analysis System: Applications to Moiré Contourogram and Interferogram," *Opt. Eng.*, **21(5)**, 901-906 (1982).

### ADDITIONAL REFERENCES

- Asai, K., "Contouring Method by Moiré Holography," *Jpn. J. Appl. Phys.*, **16(10)**, 1805-1808 (1977).
- Boehnlein, A. J. and K. G. Harding, "Adaptation of a Parallel Architecture Computer to Phase Shifted Moiré Interferometry," *Proc. SPIE*, **728**, 183-193 (1986).
- Burch, J. M., "Photographic Production of Scales for Moiré Fringe Applications," in *Optics in Metrology, Brussels Colloquium, May 6-9, 1958*, P. Mollet, Ed., Pergamon Press, New York, 1960, pp. 361-368.
- Cabaj, A., G. Ranninger, and G. Windischbauer, "Shadowless Moiré Topography Using a Single Source of Light," *Appl. Opt.*, **13(4)**, 722-723 (1974).
- Chiang, F.-P., "Techniques of Optical Signal Filtering Parallel to the Processing of Moiré-Fringe Patterns," *Exp. Mech.*, 9(11), 523-526 (Nov. 1969).
- Cline, H. E., A. S. Holik, and W. E. Lorensen, "Computer-Aided Surface Reconstruction of Interference Contours," *Appl. Opt.*, **21(24)**, 4481-4488 (1982).
- Cline, H. E., W. E. Lorensen, and A. S. Holik, "Automatic Moiré Contouring," *Appl. Opt.*, **23(10)**, 1454-1459 (1984).
- Gilbert, J. A., T. D. Dudderar, D. R. Mathtys, H. S. Johnson, and R. A. Franzel, "Two-Dimensional Stress Analysis Combining High-Frequency Moiré Measurements with Finite-Element Modeling," *Exp. Tech.*, **11(3)**, 24-28 (March 1987).
- Halioua, M., R. S. Krishnamurthy, H.-C. Liu, and F. P. Chiang, "Automated 360° Profilometry of 3-D Diffuse Objects," *Appl. Opt.*, **24(12)**, 2193-2196 (1985).
- Harding, K. G., M. Michniewicz, and A. J. Boehnlein, "Small Angle Moiré Contouring," *Proc. SPIE*, **850**, 166-173 (1987).
- Idesawa, M., T. Yatagai, and T. Soma, "Scanning Moiré Method and Automatic Measurement of 3-D Shapes," *Appl. Opt.*, **16(8)**, 2152-2162 (1977).
- Indebetouw, G., "A Simple Optical Noncontact Profilometer," *Opt. Eng.*, **18(1)**, 63-66 (1979).
- Jaerisch, W. and G. Makosch, "Optical Contour Mapping of Surfaces," *Appl. Opt.*, **12(7)**, 1552-1557 (1973).
- Kobayashi, A., Ed., *Handbook on Experimental Mechanics*, Prentice-Hall, Englewood Cliffs, NJ, 1987.



- Kujawinska, M., "Use of Phase-Stepping Automatic Fringe Analysis in Moiré Interferometry," *Appl. Opt.*, 26(22), 4712-4714 (1987).
- Miles, C. A. and B. S. Speight, "Recording the Shape of Animals by a Moiré Method," *J. Phys. E., Sci. Instrum.*, 8(9), 773-776 (1975).
- Pekelsky, J. R., "Automated Contour Ordering for Moiré Topograms," *Opt. Eng.*, 26(6), 479-486 (1987).
- Reid, G. T., "A Moiré Fringe Alignment Aid," *Opt. Lasers Eng.*, 4(2), 121-126 (1983).
- Schltzel, K. and G. Parry, "Real-Time Moiré Measurement of Phase Gradient," *Opt. Acta*, 29(11), 144-1445 (1982).
- Suzuki, M. and K. Suzuki, "Moiré Topography Using Developed Recording Methods," *Opt. Lasers Eng.*, 3(1), 59-64 (1982).
- Theocaris, P. S., "Isopachic Patterns by the Moiré Method," *Exp. Mech.*, 4(6), 153-159 (1964).
- Toyooka, S. and Y. Iwaasa, "Automatic Profilometry of 3-D Diffuse Objects by Spatial Phase Detection," *Appl. Opt.*, 25(10), 1630-1633 (1986).
- Varman, P. O., "A Moiré System for Producing Numerical Data for the Profile of a Turbine Blade Using a Computer and Video Store," *Opt. Lasers Eng.*, 5(2), 41-58 (1984).
- Yatagai, T. and M. Idesawa, "Automatic Fringe Analysis for Moiré Topography," *Opt. Lasers Eng.*, 3(1), 73-83 (1982).